



ELSEVIER

Contents lists available at ScienceDirect

Thin-Walled Structures

journal homepage: [www.elsevier.com/locate/tws](http://www.elsevier.com/locate/tws)

Full length article

## Blast loading of bumper shielded hybrid two-core Miura-ori/honeycomb core sandwich plates

Anup Pydah, R.C. Batra\*

Department of Biomedical Engineering and Mechanics, M/C 0219, Virginia Polytechnic Institute and State University, Blacksburg, VA 24061, USA



## ARTICLE INFO

## Keywords:

Miura-ori core  
Honeycomb core  
Blast mitigation  
Whipple shield  
Elastic-plastic material  
Transient deformations  
Bumper

## ABSTRACT

We analyze transient elasto-plastic deformations of two-core sandwich plates with and without a bumper and subjected to blast loads with the objective of ascertaining the energy dissipated due to plastic deformations. The facesheets and the core are assumed to be made of a high strength steel modeled as an isotropic material that obeys the von Mises yield criterion with linear strain hardening. It is first shown that considering a material failure criterion and deleting failed elements does not noticeably affect the energy dissipated in a sandwich plate. Subsequent analyses of two-core structures with and without a blast shield ignore the material failure and assume facesheets to be perfectly bonded to the core. The nonlinear transient problems have been numerically analyzed with the commercial finite element software, ABAQUS/ Explicit. Four different two-core sandwich plates obtained by varying locations of the Miura-ori and honeycomb cores are considered. Results without a shield indicate that using a Miura-ori core beneath the topmost facesheet dissipates more energy for moderate blast loads, while a combination of a honeycomb and a Miura-ori core has the least facesheet deflections. The effects of using a blast shield or a bumper, at a fixed standoff distance from a honeycomb-Miura sandwich panel, is studied by ensuring that the shield and the sandwich structure combination has the same areal density as the sandwich panel without the shield. It is found that for a given blast load, using the shield significantly reduces the energy dissipated in the sandwich panel, the bottom facesheet maximum centroidal deflection and the maximum plastic strain in the cores when compared with equal-weight panels without a shield. For the same energy dissipation, the structure with a blast shield has approximately 42% less weight than that without the shield.

## 1. Introduction

Sandwich panels are widely used as primary load bearing members in high-performance aerospace, naval and automobile industries because of their multi-functionality, high stiffness-to-weight ratios and their capability to be tailored to meet design requirements. Discrete or cellular sandwich cores, constructed as a corrugated sheet or square/hexagonal cell honeycombs, dissipate a significant amount of incident energy through a combination of their plastic compression, and bending and transverse shear deformations of the core [1], making them ideally suited for blast-mitigating applications.

The mechanical response of *single* cellular-core sandwich structures subjected to air or underwater blast loads has been investigated using both, homogenized [2–5] and discrete core models [6–16]. These studies have established that sandwich structures have higher specific energy dissipation than solid plates of the same areal density, and have indicated the superiority of the honeycomb core architecture over other core geometries [17]. However, moisture accumulation in sealed

honeycomb cells can severely compromise their mechanical performance. Novel core architectures [18–22], including origami-based designs, can help mitigate this problem and further improve the performance of sandwich structures.

Investigations on quasi-static deformations of single Miura-ori sandwich cores [23,24] and on transient deformations of blast-loaded stacked Miura-ori core sandwich beams [25] have shown the effectiveness of the Miura-ori core architecture. Design studies on single-core Miura-ori and honeycomb core sandwich plates subjected to high-intensity dynamic loads [26] have found that the Miura-ori core consistently outperforms the honeycomb core of equal areal density in terms of the energy dissipated through plastic deformations, particularly for moderate blast intensities.

*Dual-core or multi-core* sandwich panels consisting of two or more cores separated by metallic or composite facesheets have been shown to be superior to equal areal density single-core structures in terms of their impact resistance [27,28], energy absorption [29] and sound-absorbing capabilities [30]. Infinitesimal elastic deformations of multilayered

\* Corresponding author.

E-mail addresses: [anpydah@vt.edu](mailto:anpydah@vt.edu) (A. Pydah), [rbatra@vt.edu](mailto:rbatra@vt.edu) (R.C. Batra).

foldcore sandwich panels have been analytically studied [31], however, the mechanics of transient deformations of the elasto-plastic core under dynamic loads [25,26] is quite involved due to inertia effects. For single core elasto-plastic sandwich plates with the Miura-ori and the honeycomb cores [26] of equal areal density with material failure not considered, we found that while the bottom facesheet of the Miura-ori core sandwich plate had lesser maximum deflection the honeycomb core considerably reduced the top facesheet maximum deflection. Furthermore, for moderate blast intensities, the Miura-ori cores dissipated a greater fraction of the incident energy through plastic deformations than the honeycomb cores.

In terms of structural reliability, an ideal sandwich panel should dissipate large quantities of energy without sacrificing its integrity. This has motivated us to study two-core sandwich plates with the Miura-ori and the honeycomb core located in either the top or the bottom layer, which gives four combinations - Miura-honeycomb, honeycomb-Miura, Miura-Miura and honeycomb-honeycomb, wherein the first term refers to the top core that first interacts with the blast load.

For space structures, a thin shield placed at a distance above the primary structure, known as a Whipple bumper [32], efficiently reduces the penetration due to hypervelocity meteoric impact and offers considerable weight savings [33–39]. For aircrafts, a Hardened Unit Load Device (HULD) [40] and an overhead bin blast composite shield [41] provide on-board countermeasures against small explosions. There is a clear need for research on shielding aircraft, automobile and naval structures from high-intensity dynamic loads caused by explosive blasts or crashes.

Thus, objectives of this paper are to:

1. Examine effects of a Whipple shield, i.e., a thin metallic plate located above the primary structure and interacting first with the blast load.
2. Delineate effects of considering material failure and deleting failed elements from the analysis.
3. Investigate the blast performance of hybrid two-core sandwich structures designed as a combination of Miura-ori and square honeycomb core layers perfectly bonded to facesheets.

The finite element (FE) software ABAQUS/ Explicit ver. 6.14 [42] is used to numerically solve the pertinent nonlinear initial-boundary-value elastic-plastic problems by using the FE mesh that gave converged results for a prototype one-core sandwich structure. It is found that considering a damage model and deleting failed elements has a minimal effect on the energy absorbed and the maximum deflection of the structure. Material strain rate effects, thermal softening, debonding between the core and the facesheets and imperfections, if any, in the cores have not been considered.

Design studies conducted to investigate the influence of the unit cell parameters of the Miura-ori and the honeycomb pattern on the sandwich panel deformations indicate that design trade-offs need to be considered. The Miura-ori core in the top layer dissipates more energy through plastic deformations, and the honeycomb-Miura combination minimizes the facesheet deflections. Using a panel with a Whipple shield reduces the back facesheet maximum deflection and decreases the maximum equivalent plastic strain in the cores when compared with an equal areal density panel without the shield. For the same energy dissipation under a given blast load, the structure with a blast shield has approximately 42% less weight than that without the shield.

The layout of the remainder of the paper is as follows. The geometry of the two-core Miura-ori and honeycomb sandwich plate, the constitutive relations for the material and the FE modeling in ABAQUS/ Explicit are described in Section 2. Results for (i) a single-layer sandwich plate under blast loads with and without considering material failure, and (ii) a single fold with and without accounting for pre-damage induced in its crease during the fabrication process are also discussed in Section 2. The collapse kinematics and the response of the

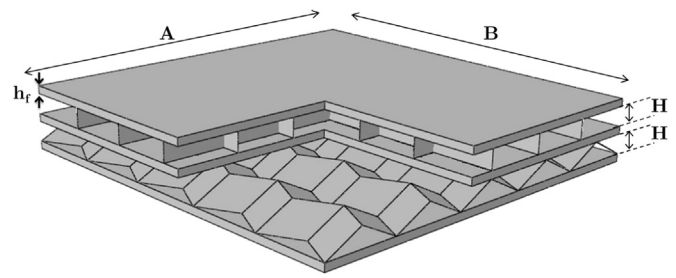


Fig. 1. “Honeycomb-Miura” hybrid sandwich plate.

four two-core sandwich plates under blast loads are described in Section 3. The influence of unit cell parameters on the energy dissipated due to plastic deformations in the cores and on the facesheet deflections of the two-core sandwich plates are presented in Section 4. The influence of a blast shield on deformations of a honeycomb-Miura sandwich plate is examined in Section 5. In Section 6 we comment upon experimental work needed to verify results of simulations. Conclusions of the work are summarized in Section 7.

## 2. Geometry and modeling of the hybrid two-core sandwich plate

The hybrid two-core sandwich plate consists of a top, a middle, and a bottom facesheet with two cores (of either a Miura-ori or a honeycomb-type architecture) between a pair of facesheets (see, for example, Fig. 1, for the “honeycomb-Miura” combination). The three facesheets, assumed here to be identical for simplicity, have dimensions  $A \times B \times h_f$  and the core thickness equals  $H$ . The edges of the facesheets are rigidly clamped and a high-intensity dynamic load given by

$$p(r, t) = \begin{cases} 0 & t < t_a \\ p(t)e^{-(r/r_0)^2} & t \geq t_a \end{cases} \quad (1)$$

where

$$p(t) = P_0 \left[ 1 - \frac{t - t_a}{t_d} \right] e^{-(t-t_a)/t_\theta} \quad (2)$$

is applied to the outer surface of the top facesheet. The blast pressure is adapted from the numerical studies of Dharmasena et al. [9], and exponentially decreases with distance  $r$  from the facesheet centroid according to Eq. (1). The peak overpressure  $P_0$  occurs at  $r = 0$  and time  $t = t_a$  and decreases exponentially with time  $t > t_a$  (see Fig. 2). We set,  $r_0 = 50$  mm,  $t_a = 20$   $\mu$ s,  $t_d = 180$   $\mu$ s and  $t_\theta = 189.8$   $\mu$ s. Batra and Hassan [43] considered  $p$  to be a polynomial of degree 4 in  $r$  and exponentially decaying in time with various parameters given by Cole's [44] empirical formulae.

The Miura-ori core consists of  $x_m$  and  $y_m$  “unit cells” tessellated along and across the corrugation, respectively. A single unit cell is constructed from four identical parallelograms which can be characterized by four parameters in its unfolded state: side lengths  $a$  and  $b$ ,

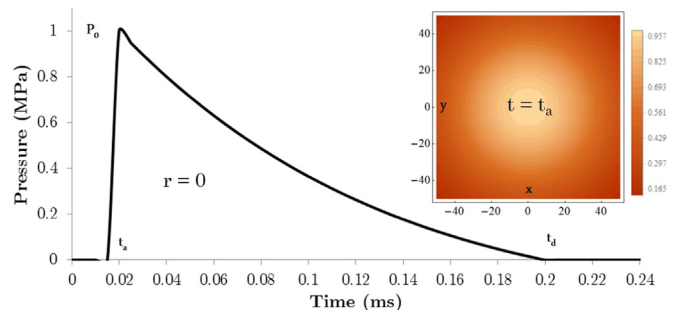


Fig. 2. Time and spatial (inset) variation of the high-intensity dynamic load (Eq. (2)).

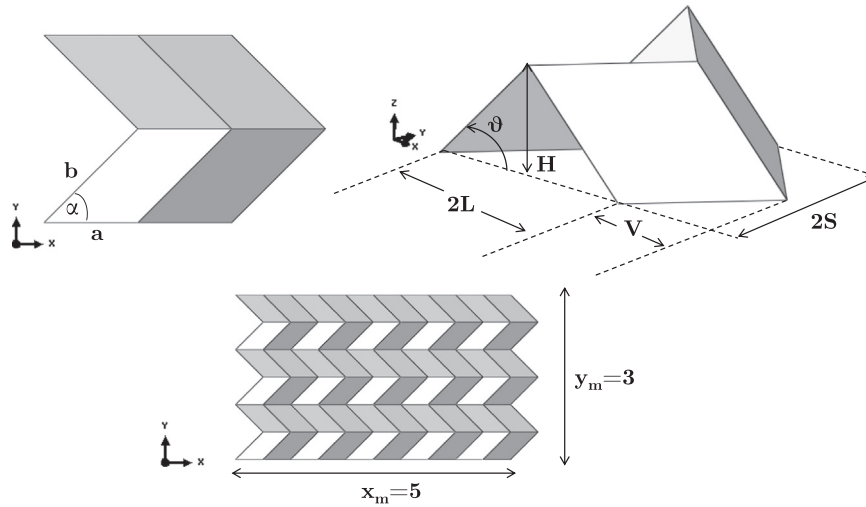


Fig. 3. Geometric parameters of a Miura-ori unit cell.

acute angle  $\alpha$  and the sheet thickness  $t_s$  (Fig. 3). In a particular folded configuration, the Miura-ori unit cell requires an additional parameter, the dihedral fold angle  $\theta$  between the facets and the horizontal base, to completely characterize the core. Alternatively, a unit cell can also be described by its outer dimensions, height  $H$ , width  $2S$ , length,  $2L$ , and amplitude  $V$  given by [45]

$$H = a \sin \theta \sin \alpha, \quad S = b \frac{\cos \theta \tan \alpha}{\sqrt{1 + \cos^2 \theta \tan^2 \alpha}} \quad (3)$$

$$L = a \sqrt{1 - \sin^2 \theta \sin^2 \alpha}, \quad V = b \frac{1}{\sqrt{1 + \cos^2 \theta \tan^2 \alpha}} \quad (4)$$

The relative mass density,  $\rho_c$ , of the Miura-ori core is given by

$$\rho_c = \frac{a b t_s \sin \alpha}{H S L} \rho_m \quad (5)$$

where  $\rho_m$  is the mass density of the core material.

The square honeycomb core consists of a set of orthogonal webs  $(x_m, y_m)$  of height  $H$  and thickness  $t_w$  running in the  $x$ - and the  $y$ -directions.

The relative mass density,  $\rho_c$ , of the honeycomb core is given by

$$\rho_c = \frac{(x_m + y_m)t_w}{a} \rho_m \quad (6)$$

The dimensions of the Miura-ori unit cell are chosen as  $a = b = 11.18$  mm,  $\alpha = 66.42$  deg,  $t_s = 0.218$  mm, and  $H = 5$  mm. This results in a Miura-ori core with  $\{x_m, y_m\} = \{5, 5\}$  and the dihedral angle  $\theta = 29.21$  deg. For the honeycomb core, a grid of 25 webs with  $\{x_m, y_m\} = \{5, 5\}$  is chosen with  $t_w = 0.5$  mm and  $H = 5$  mm. In order to compare the performance of the Miura-ori and the square honeycomb cores of equal areal density, the facesheet dimensions were fixed at  $100 \times 100 \times 2$  mm and the core density at approximately  $0.05\rho_m$ .

### 2.1. Material parameters

The facesheets and the cores are made of the same homogeneous, isotropic, bilinear elastic-plastic material that obeys the von Mises yield criterion with isotropic hardening that is representative of a High Strength Low Alloy steel HSLA-65. We set  $\rho_m = 7800$  kg m<sup>-3</sup>, Young's modulus  $E = 200$  GPa, Poisson's ratio  $\nu = 0.3$ , yield stress  $\sigma_y = 300$  MPa and the hardening tangent modulus  $E_t = 2$  GPa.

For studying material failure, we use the Johnson-Cook failure criterion [46] included in ABAQUS 6.14 [42]. Damage is assumed to initiate when

$$\sum \frac{\Delta \bar{\epsilon}^{pl}}{\bar{\epsilon}_D^{pl}} = 1 \quad (7)$$

where  $\Delta \bar{\epsilon}^{pl}$  is the increment in the equivalent plastic strain and the summation is performed over all increments of loading. The equivalent plastic strain,  $\bar{\epsilon}_D^{pl}$ , is defined as

$$\bar{\epsilon}_D^{pl} = [d_1 + d_2 \exp(-d_3 \eta)] \left[ 1 + d_4 \ln \left( \frac{\dot{\bar{\epsilon}}^{pl}}{\dot{\bar{\epsilon}}_0} \right) \right] [1 + d_5 \hat{\theta}] \quad (8)$$

which accounts for effect of the stress triaxiality, strain rate, and temperature. In Eq. (8),  $d_1 - d_5$  are material parameters,  $\eta = -p/q$  is the stress triaxiality coefficient,  $p$  the hydrostatic pressure (negative in tension),  $q$  the von Mises equivalent stress,  $\dot{\bar{\epsilon}}^{pl}$  the equivalent plastic strain rate,  $\dot{\bar{\epsilon}}_0$  the reference strain rate and  $\hat{\theta}$  is the non-dimensional temperature defined as

$$\hat{\theta} = \begin{cases} 0 & \theta < \theta_{\text{transition}} \\ (\theta - \theta_{\text{transition}})/(\theta_{\text{melt}} - \theta_{\text{transition}}) & \theta_{\text{transition}} \leq \theta \leq \theta_{\text{melt}} \\ 1 & \theta > \theta_{\text{melt}} \end{cases} \quad (9)$$

Here  $\theta$ ,  $\theta_{\text{melt}}$  and  $\theta_{\text{transition}}$  are, respectively, the current, the melting and the transition temperatures. Upon the damage onset, Young's modulus is degraded by  $(1 - D)$  with the damage variable  $D$  computed from

$$\dot{D} = \frac{\bar{u}_f^{pl}}{\bar{u}_f^{pl}} \quad (10)$$

where  $\bar{u}_f^{pl}$  is the effective plastic displacement at the point of failure and is introduced to reduce the mesh dependency of the computed results. The value of  $\bar{u}_f^{pl}$  can be directly specified by the user or given in terms of the fracture energy dissipated per unit area,  $G_f$ , as  $\bar{u}_f^{pl} = \frac{2G_f}{\sigma_y}$  where  $\sigma_y$  is the current yield stress. The element is deleted from the analysis domain when  $D = 1$  at one of its integration points. Setting  $\bar{u}_f^{pl} = 0$  implies instantaneous failure of the element when Eq. (7) holds.

We set  $d_1 = 0.05$ ,  $d_2 = 3.44$ ,  $d_3 = 2.12$  and  $d_4 = d_5 = 0$  which is representative of a 4340 Steel [46] with the assumption of neglecting strain rate and temperature effects. Results are computed for a range of values of  $\bar{u}_f^{pl}$ .

The structure is assumed to be initially at rest and stress free.

### 2.2. FE meshes

The facesheets of the sandwich plate were discretized using eight-node C3D8R brick elements with reduced integration into  $60 \times 60 \times 3$  uniform elements. The Miura-ori and the honeycomb cores were meshed using four-node S4R shell elements with reduced integration. Each

**Table 1**

Results at  $t = 3$  ms for 4 FE meshes for the Miura-ori core with  $\{x_m, y_m\} = \{5, 5\}$  and  $H = 10$  mm.

Miura-ori facet mesh density	PD <sup>*</sup> core (kJ)	$\epsilon_p$	Deflection (mm)	
			Bottom	Top
10 × 10	0.394	0.782	15.13	19.72
15 × 15	0.423	0.987	14.84	19.50
20 × 20	0.427	1.108	14.93	19.68
25 × 25	0.427	1.112	14.94	19.68

\*PD = Energy dissipated due to plastic deformations.

parallelogram facet of the Miura-ori core was meshed with  $20 \times 20$  uniform elements while each web of the honeycomb core was meshed with 20 uniform elements along its depth and 60 uniform elements along its length. In Ref. [26] we showed that results for shock loads using these shell elements and the C3D8R elements for the core were virtually identical to each other.

To simulate perfect bonding, the cores were attached to the facesheets using the tie constraint. The general contact algorithm in ABAQUS was used to ensure frictionless contact and non-interpenetration between surfaces that may contact each other during the deformation process.

**2.3. Mesh convergence study**

We computed the response of a single-core Miura-ori sandwich plate with  $\{x_m, y_m\} = \{5, 5\}$ ,  $H = 10$  mm subjected to a blast load given by Eq. (1) with  $P_0 = 100$  MPa applied to the outer surface of the top facesheet. We used mesh densities ranging from  $10 \times 10$  (14, 400 total) to  $25 \times 25$  (78, 400 total) elements in each core facet. For the facesheets, we used  $60 \times 60 \times 3$  uniform elements. Key results presented in Table 1 at  $t = 3$  ms indicate that the global response quantities like the maximum equivalent plastic strain in the core,  $\epsilon_p$ , and the energy dissipated due to plastic deformations, PD, in the core as well as local quantities like the centroidal deflections of the facesheets, converged for the  $20 \times 20$  FE mesh in a core facet. For all numerical simulations in this paper, we have used  $20 \times 20$  uniform elements in each Miura-ori core facet and  $20 \times 60$  uniform elements for each web of the honeycomb core for which results with different meshes were not computed.

**2.4. Comparison of results with and without considering material failure**

For  $P_0 = 100$  and 300 MPa in Eq. (1), and a range of values of  $\bar{u}_f^{pl}$ , the computed results at  $t = 3$  ms are listed in Table 2. These reveal that for  $P_0 = 100$  MPa, there is a minimal influence of the  $\bar{u}_f^{pl}$  value on the

**Table 2**

Effect of  $\bar{u}_f^{pl}$  on the energy dissipated due to plastic deformations and facesheet deflections of the single-layered Miura-ori sandwich plate with  $\{x_m, y_m\} = \{5, 5\}$  and  $H = 5$  mm.

$P_0$ (MPa)	$\bar{u}_f^{pl}$ (mm)	PD core (kJ)	Total PD (kJ)	Bottom facesheet deflection (mm)	Top facesheet deflection (mm)
100	0	0.425	1.823	14.85	19.67
	0.001	0.425	1.823	14.87	19.69
	0.01	0.425	1.823	14.87	19.69
	0.1	0.425	1.823	14.87	19.69
	1	0.425	1.823	14.87	19.69
	10	0.425	1.823	14.87	19.69
	300	0	1.773	14.711	44.08
0.001		1.774	14.711	44.06	46.78
0.01		1.764	14.708	43.78	46.70
0.1		1.715	14.690	42.39	46.34
1		1.729	14.632	41.02	46.08
10		1.874	14.604	40.51	45.68

**Table 3**

Effect of including a damage and a failure model on the energy dissipated due to plastic deformations and facesheet deflections of the single-layered Miura-ori sandwich plate with  $\{x_m, y_m\} = \{5, 5\}$  and  $H = 5$  mm .

$P_0$ (MPa)	Case	PD core (kJ)	Total PD (kJ)	Bottom facesheet deflection (mm)	Top facesheet deflection (mm)
50	ND <sup>*</sup>	0.167	0.506	6.64	11.24
	D <sup>**</sup>	0.167	0.506	6.64	11.24
100	ND	0.394	1.793	14.90	19.69
	D	0.425	1.823	14.85	19.67
200	ND	1.099	6.682	28.15	33.07
	D	1.049	6.667	28.50	33.22
300	ND	1.752	14.493	40.05	45.31
	D	1.773	14.711	44.08	46.79

\*ND = No damage and failure considered; D<sup>\*\*</sup> = Element failed when Eq. (7) holds.

energy dissipated due to plastic deformations in the structure and the facesheet deflections. For  $P_0 = 300$  MPa, the energy dissipated and the top facesheet deflections are little changed when  $\bar{u}_f^{pl}$  is increased from 0 to 0.01 mm. For subsequent increase in the  $\bar{u}_f^{pl}$  value to 10 mm, the four quantities listed in the Table change by at most 8%.

In Table 3, we have compared results of the energy dissipation and the facesheet deflections with  $\bar{u}_f^{pl} = 0$  (i.e., instantaneous material failure upon satisfaction of Eq. (7) and ignoring the material failure. Clearly, the energy dissipation and the facesheet deflections are relatively unaffected by considering material failure for  $P_0 \leq 200$  MPa. Similar observations are noted for the equivalent plastic strain and the transverse displacement of the Miura-ori core for  $P_0 = 200$  MPa in Figs. 4 and 5 which show fringe plots of the equivalent plastic strain and the transverse displacement. Failure initiates at  $t = 0.165$  ms at the folds running along the  $y$ - axis near the center and edges of the core and results in elements being deleted along the fold lines. When the material failure is ignored, the equivalent plastic strain in these critical locations (shown in black) increases beyond the values included in the legend.

**2.5. Sensitivity of results to minute variations in the peak load**

It is reported in Refs. [47–50] that a tiny change in the impact speed can significantly affect some results for the hypervelocity impact on a fused glass plate. In Table 4, we list the energy dissipation and the facesheet deflections for  $\Delta P_0 = \pm 0.01$  MPa around  $P_0 = 100$  and 300 MPa. It is evident that values of the four variables listed in Table 4 are essentially unaffected by a  $\pm 0.01\%$  change in  $P_0$ . We note that material failure including crack initiation and propagation was considered (a tiny particle impacting a homogeneous plate and forming a crater) in Ref. ([47]), while for this numerical experiment  $\bar{u}_f^{pl} = 0$ , which implies material failure when Eq. (7) is satisfied and the target is a sandwich structure.

**2.6. Effect of crease weakening due to folding**

In order to delineate the effect of the weakening of the crease due to the folding of the core from a sheet metal on the energy dissipated in the core, we modeled a single 90 deg fold of thickness 0.35 mm sandwiched between two rigid plates  $H = 10$  mm apart and very long in the  $y$ - direction (plane strain deformations). Along the regions abutting the crease (shown in red in Fig. 6), we degraded the yield stress,  $\sigma_y$ , of the material from 300 MPa to 200 MPa to simulate the weakening of the crease. The top facesheet is suddenly moved downwards with velocity  $v_0 = 10$  m/s, while the bottom facesheet is rigidly fixed, which mimics a blast loading scenario. The degraded (intact) region in each web of the fold was meshed with 10 (100) uniform shell elements along its length. The Johnson-Cook damage criterion (Eqs. (7) and (8)) with  $\bar{u}_f^{pl} = 0$  was used to model material failure. In Table 5 we have compared the energy

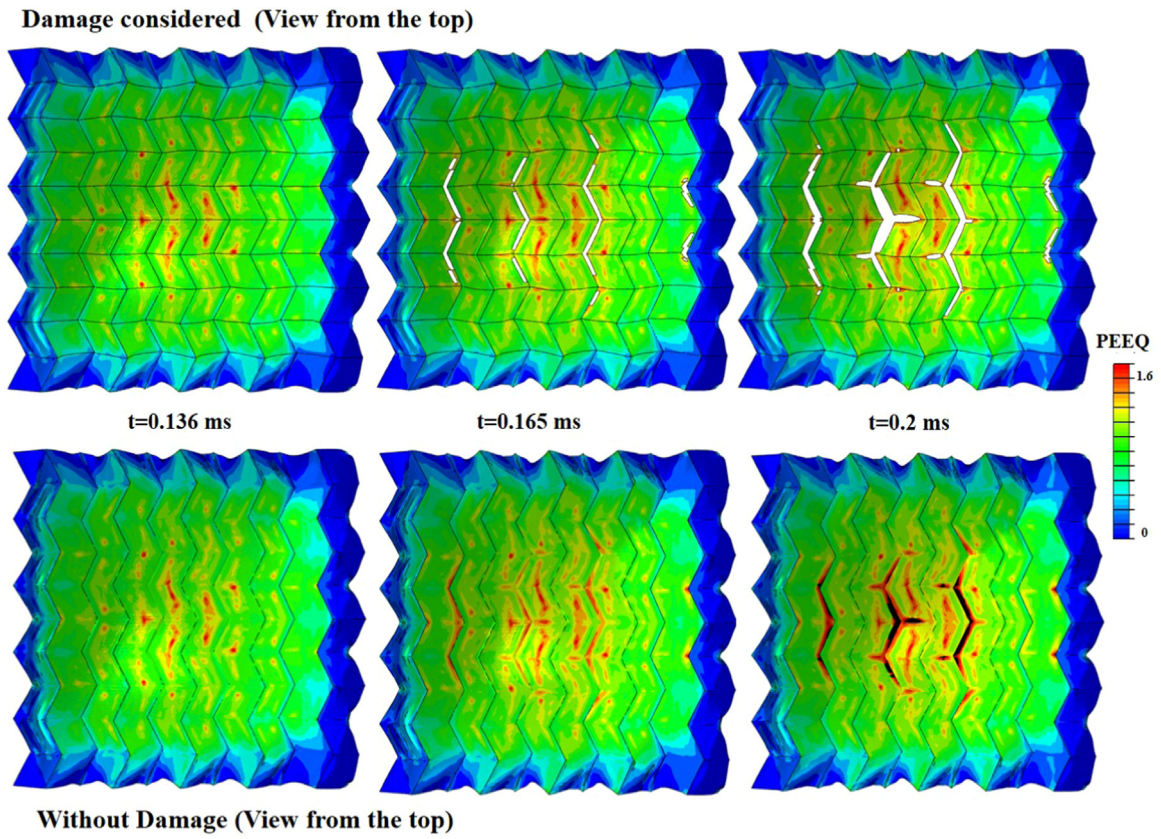


Fig. 4. Effect of consideration of damage on the equivalent plastic strain (PEEQ) in the Miura-ori core at three times for  $P_0 = 200$  MPa.

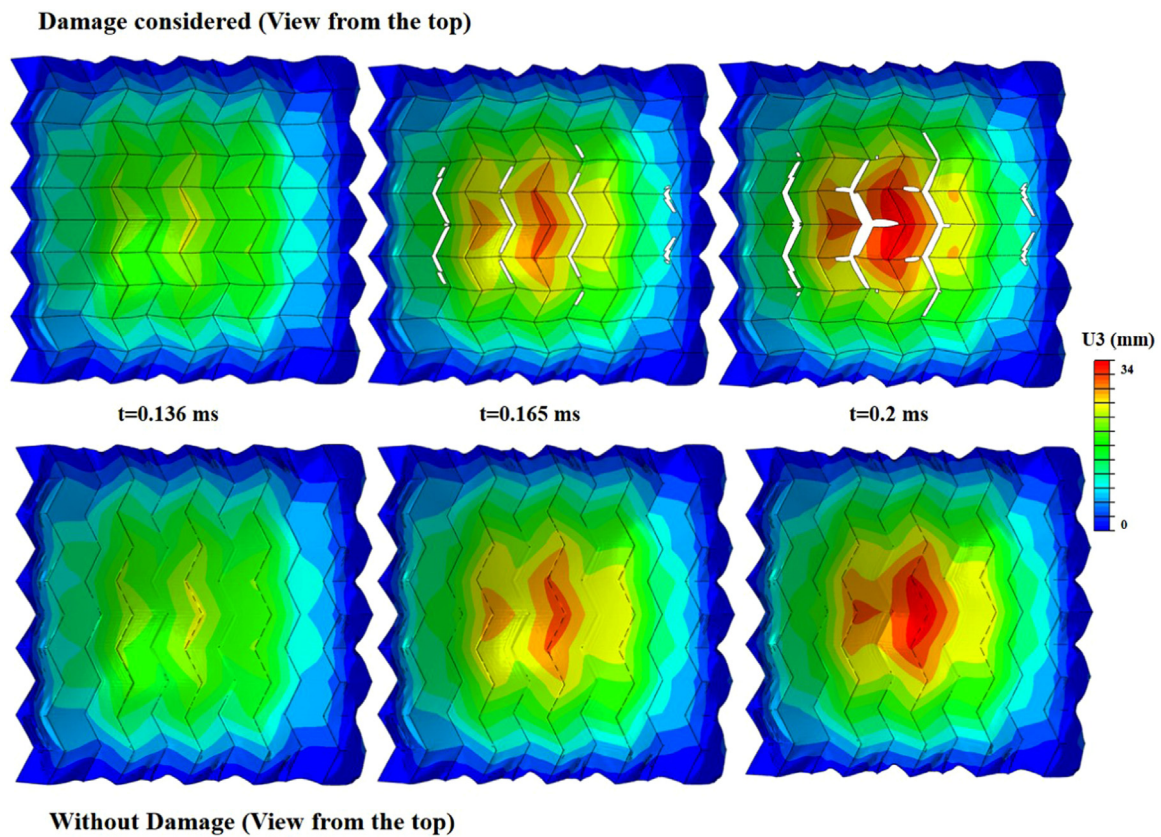
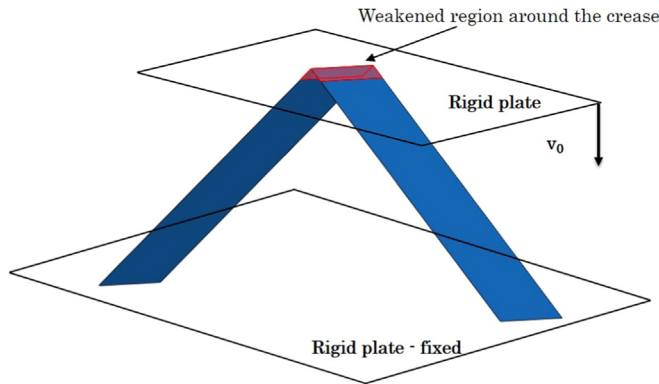


Fig. 5. Effect of consideration of damage on the transverse displacement ( $u_3$ ) in the Miura-ori core at three times for  $P_0 = 200$  MPa.

**Table 4**  
Sensitivity of results to minute variations in the peak load  $P_0$  for the single-layered Miura-ori sandwich plate with  $\{x_m, y_m\} = \{5, 5\}$ ,  $H = 5$  mm and  $\bar{u}_j^{pl} = 0$ .

$P_0$ (MPa)	PD core (kJ)	Total PD (kJ)	Bottom facesheet deflection (mm)	Top facesheet deflection (mm)
99.99	0.4246	1.8229	14.8517	19.6837
100	0.4247	1.8233	14.8525	19.6699
100.01	0.4248	1.8235	14.8504	19.6747
299.99	1.7715	14.7101	44.0962	46.7991
300	1.7733	14.7110	44.0812	46.7886
300.01	1.7721	14.7130	44.0912	46.8027



**Fig. 6.** Crushing test on a 90 deg fold with a weakened crease region. (For interpretation of the references to color in this figure legend, the reader is referred to the web version of this article.)

**Table 5**  
Effect of weakening of the crease for a 90 deg fold with  $v_0 = 10$  m/s and  $\bar{u}_j^{pl} = 0$ .

Case	PD crease (J)	PD rest of fold (J)	$\epsilon_p$
Crease weakening	0.13	2.36	0.45
No crease weakening	0.09	2.20	0.39

dissipated due to plastic deformations in the crease region and the rest of the fold as well as the maximum equivalent plastic strain,  $\epsilon_p$ , with and without crease weakening. We note that the contribution of the crease (and the abutting regions) to the total energy dissipated by the fold is not significant ( $\sim 5\%$ ). However, weakening the crease increases the maximum equivalent plastic strain by about 23%, which indicates that failure could occur earlier in the deformation process.

In order to economize on computational resources, we do not consider material failure and crease weakening in the results reported and discussed below.

### 3. Dynamic response of hybrid two-core sandwich plates

The blast response of the Miura-honeycomb, honeycomb-Miura, Miura-Miura and honeycomb-honeycomb sandwich plates was analyzed. The facesheet and the core dimensions are the same as those mentioned in the previous section. Fig. 7 shows the computed deformed shapes at  $t = 3$  ms of the honeycomb-Miura sandwich panel and centrally situated Miura-ori and honeycomb unit cells for  $P_0 = 100$  MPa. Some portions of the facesheets have been deleted to evince deformations of the core webs. For the Miura-ori core, the mountain folds on top of the facets tend to flatten, fold, bend inwards and get compacted, while for the honeycomb core, the primary deformation mode is plastic buckling, mostly confined to the upper segment of the webs, consistent with previous findings [4]. For transient bending deformations of a thin rectangular plate and a thin circular cylinder made of a

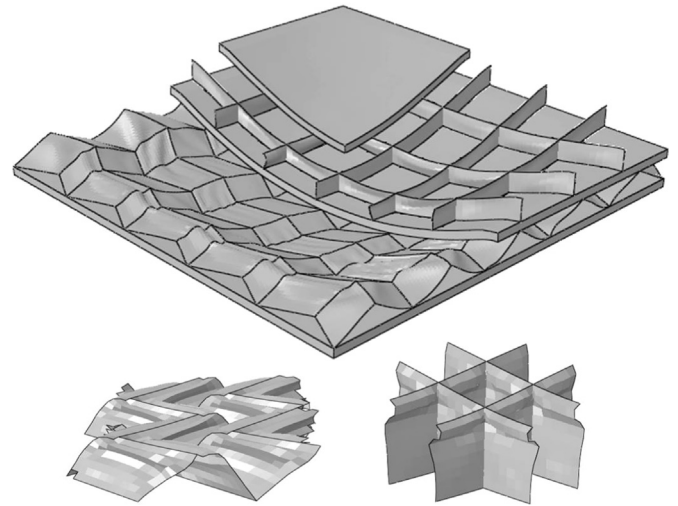


**Fig. 7.** Deformed shape of the honeycomb-Miura hybrid sandwich plate and centrally situated Miura-ori and honeycomb unit cells.

thermoviscoplastic material with elastic deformations neglected, Batra and Wei [51,53] found that the imposed axial strain rate and the plate thickness/side length strongly influenced the buckled shape of the plate, and of the cylinder.

The computed work done by the applied pressure field at  $t = 3$  ms equaled 1.264 kJ while the sum of the kinetic energy (0.6 J), the elastic strain energy (7.6 J) and the energy dissipated due to plastic deformations (1.187 kJ) equals 1.195 kJ. Thus the energy dissipated due to the numerical integration scheme employed and the hour glass modes that could be induced by the reduced integration was 5.4% of the work done by the applied pressure.

For each of the four core combinations, time histories ( $0 \leq t \leq 0.3$  ms) of the vertical displacement and the vertical velocity of the centroidal node at the bottom of each facesheet, the total kinetic energy, the energy dissipated in the sandwich plate and the work done by the blast load on the structure are shown in Figs. 8–14. We have also depicted time histories of the *centroidal core compression* that equals the difference between the central deflection of the bottom surface of the top facesheet and that of the top surface of the middle facesheet for the top core. The bottom core compression is similarly defined. Three phases of the response, namely, the centroidal core compression (I), the overall panel bending and stretching (II), and elastic oscillations (III), similar to those detailed in Ref. [26] for single-core Miura-ori sandwich plates, are observed. However, each of the four combinations exhibit qualitatively different behaviors discussed below.

#### 3.1. The honeycomb-Miura combination (Figs. 8 and 9)

1. Core compression ( $0 < t < 0.11$  ms): Due to negligible compression of the honeycomb core centroid, the top and the middle facesheet centroidal points move together leading to a rapid equalization of their velocities at approximately  $t = 0.04$  ms while the bottom facesheet remains stationary till  $t = 0.03$ ms. The Miura-ori core gets compressed to its maximum value of 5 mm at  $t = 0.11$  ms and helps restrict the maximum kinetic energy imparted by the blast (see Fig. 9). Upon complete densification of the Miura-ori core, the core height reduces to approximately 0, the middle facesheet “slaps” against the bottom facesheet at  $t = 0.09$  ms transferring a part of its linear momentum that suddenly increases the bottom facesheet velocity to approximately 90 m/s.
2. Panel bending and stretching ( $0.11 < t < 0.22$  ms): With the facesheet edges clamped, the entire sandwich plate bends elasto-plastically that reduces velocities of the three facesheets which reach their points of maximum permanent deflection at  $t = 0.22$  ms. After the

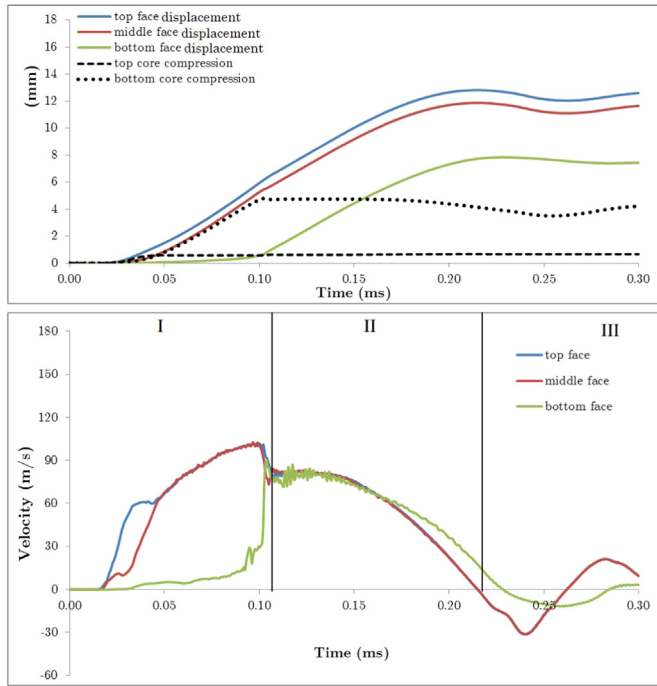


Fig. 8. Time evolution of the centroidal velocities and displacements of the facesheets for the honeycomb-Miura combination.

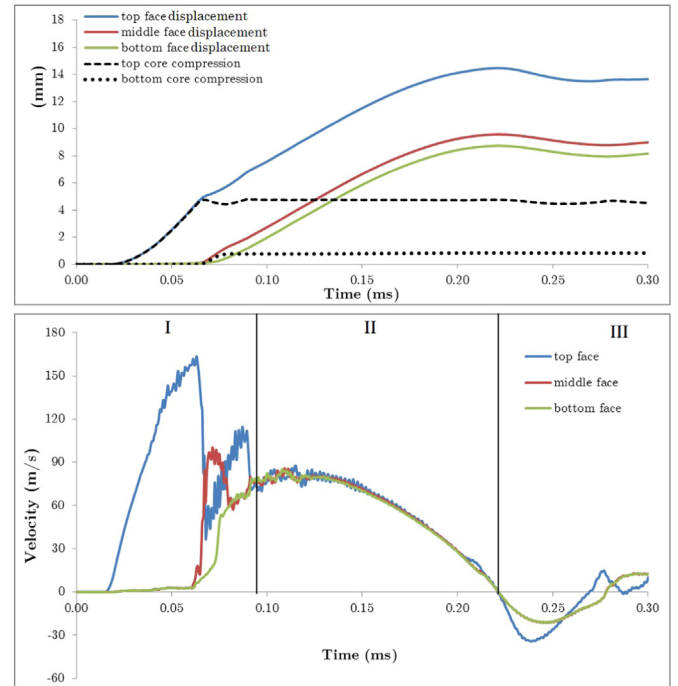


Fig. 10. Time evolution of the centroidal velocities and displacements of the facesheets for the Miura-honeycomb combination.

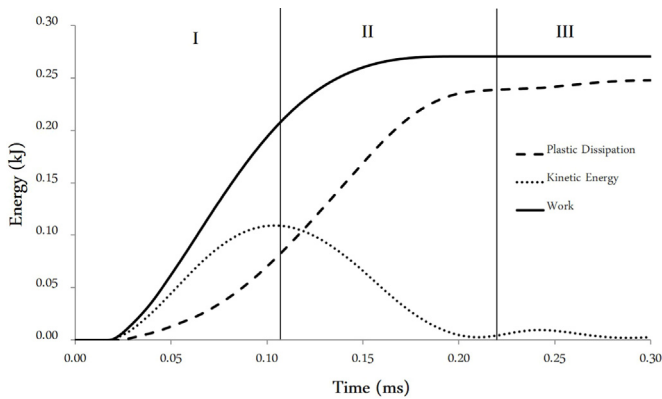


Fig. 9. Time histories of the total kinetic energy, the total plastic dissipation in the honeycomb-Miura sandwich plate, and of the work done by the blast load.

faceslap at  $t = 0.11$  ms the Miura-ori core springs back, the bottom core centroidal compression reduces and breaks the synchronous motion of the three facesheets at  $t = 0.17$  ms. However, the top and the middle facesheet centroids continue to move together at a velocity lower than that of the bottom facesheet centroid which then decelerates to 0 at  $t = 0.22$  ms.

3. Elastic oscillations about the final deflected state ensue that die out at approximately 3 ms (not shown in the figure) due to structural plastic deformations.

### 3.2. The Miura-honeycomb combination (Figs. 10 and 11)

1. Centroidal core compression ( $0 < t < 0.09$  ms): The middle facesheet remains essentially stationary till  $t = 0.07$  ms as the top facesheet accelerates towards it attaining a peak velocity of approximately 175 m/s while rapidly compressing the Miura-ori core. Upon nearly complete densification of the upper core at  $t = 0.07$  ms, the top facesheet transfers its linear momentum to the middle facesheet through a faceslap resulting in a sudden drop of the top facesheet velocity and rapid acceleration of the middle facesheet. Due to

minimal compression of the lower honeycomb core, the velocities of the middle and the bottom facesheets equalize at approximately 60 m/s, at  $t = 0.08$  ms. They then move in unison away from the top facesheet which helps the upper core increase its height due to spring back ( $0.07 < t < 0.08$  ms). As the Miura-ori core regains a part of its stiffness, it pulls the top facesheet towards the combination of the middle and the bottom facesheets at  $t = 0.08$  ms and helps to equalize their velocities at approximately 75 m/s and restrict the maximum kinetic energy of the structure (see Fig. 11).

2. Panel bending and stretching ( $0.09 < t < 0.22$  ms): With minimal change in the centroidal core compressions, the entire sandwich plate moves synchronously and helps to significantly dissipate the kinetic energy of the structure through plastic bending and stretching (see Fig. 11). The facesheets reach their points of maximum permanent deflection at the end of this stage at  $t = 0.22$  ms.
3. Elastic oscillations about the final deflected state die out at approximately 3 ms (not shown in the figure) due to structural plastic deformations.

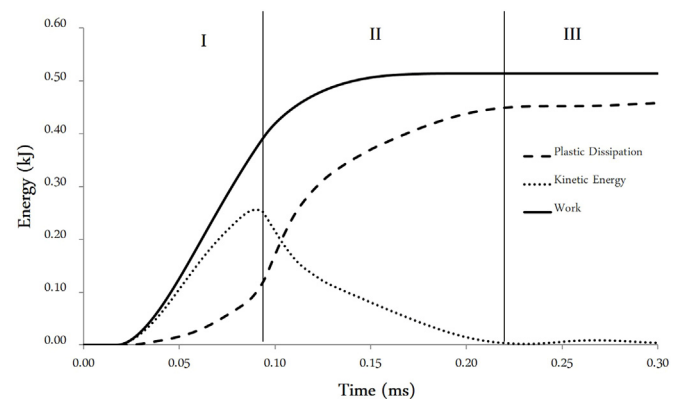


Fig. 11. Time histories of the total kinetic energy, the total plastic dissipation in the Miura-honeycomb sandwich plate, and of the work done by the blast load.

Observations from deformations of the two hybrid sandwich plate combinations are listed below:

1. Equalization of velocities of the three facesheets through a combination of the plastic core compression and linear momentum transfer helps to restrict the maximum kinetic energy of the sandwich structure.
2. For  $P_0 = 100$  MPa, the honeycomb core compression is significantly lesser than that of the Miura-ori core. This results in smaller deflections of the upper-bounding facesheet for the honeycomb core and of the lower-bounding facesheet for the Miura-ori core.
3. Using the Miura-ori core at the top, i.e., as the core that faces the blast load, can cause complete densification of the core that can result in faceslaps, high reaction forces at the supports of the facesheets and a large velocity of the upper facesheet.

3.3. The Miura-Miura (Figs. 12 and 13) and honeycomb-honeycomb (Figs. 14 and 15) combinations

The Miura-Miura combination behaves akin to the single layer Miura-ori core sandwich plate [26]: both cores are significantly compressed by  $t = 0.12$  ms and the velocity equalization occurs at  $t = 0.18$  ms through a series of faceslaps at  $t = 0.07, 0.12$  and  $0.16$  ms (see Fig. 12). Since a large fraction of the incident energy is dissipated through plastic deformations of the cores during the velocity equalization phase, ( $0 < t < 0.17$  ms, see Fig. 13), the panel bending stage (II) is much shorter ( $0.17 < t < 0.22$  ms) than that for the previous two cases.

For the honeycomb-honeycomb combination both cores do not compress significantly resulting in a rapid equalization (at  $t = 0.07$  ms) of the velocities of all three facesheets at approximately 60 m/s (see Fig. 14). Thus, a significant fraction of the incident energy is dissipated through plastic bending of the facesheets (see Fig. 15) during the panel bending stage of long duration ( $0.07 < t < 0.22$  ms). Furthermore, the maximum velocity attained by the facesheets is the least amongst those for the other three combinations.

Clearly, each two-core sandwich plate combination exhibits a

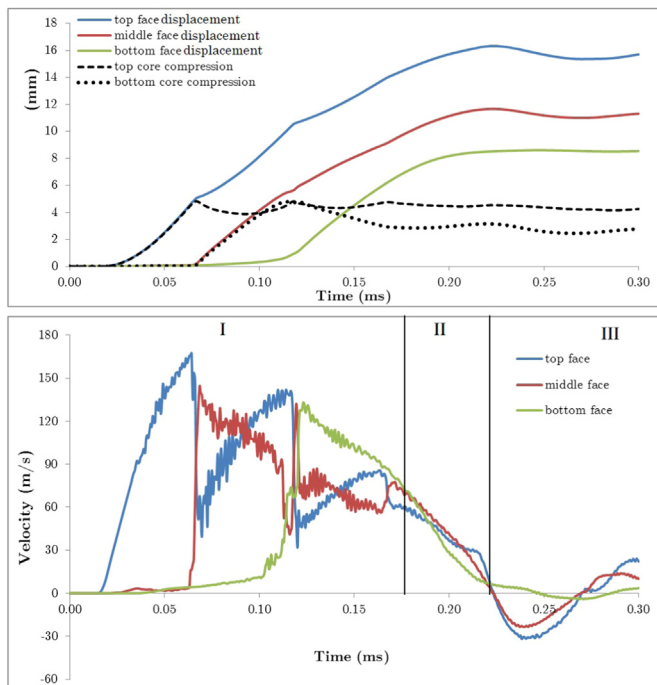


Fig. 12. Time evolution of the centroidal velocities and displacements of the facesheets for the Miura-Miura combination.

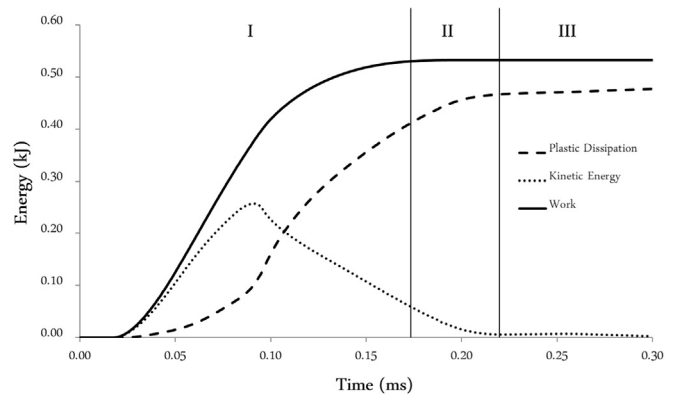


Fig. 13. Time histories of the total kinetic energy, the total plastic dissipation in the Miura-Miura sandwich plate, and of the work done by the blast load.

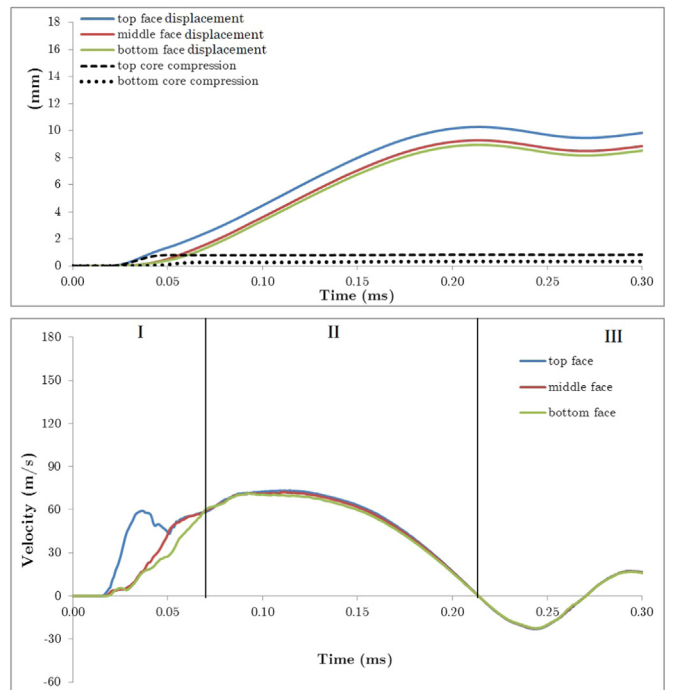


Fig. 14. Time evolution of the centroidal velocities and displacements of the facesheets for the honeycomb-honeycomb combination.

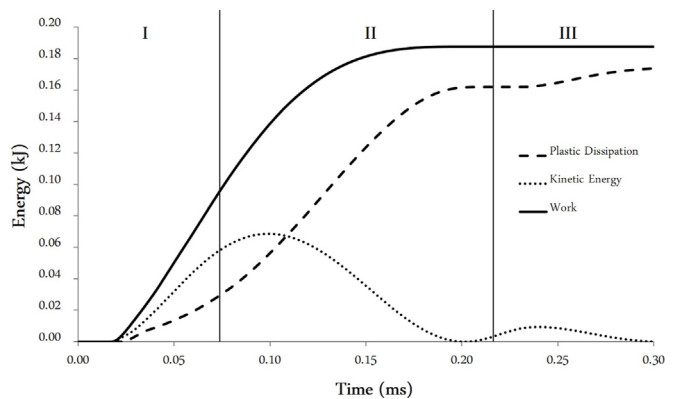


Fig. 15. Time histories of the total kinetic energy, the total plastic dissipation in the honeycomb-honeycomb sandwich plate, and of the work done by the blast load.

qualitatively different mechanical response to blast loads. In order to establish the effectiveness of each combination, the influence of the unit cell parameters of the Miura-ori and the honeycomb pattern on plastic dissipation in the cores and the facesheet deflections are investigated in the next section.

#### 4. Influence of unit cell parameters on the plastic dissipation in the cores

In our earlier work on the crush dynamics of single-layered Miura-ori sandwich plates [26], we have extensively discussed (see Section 5) the influence of the unit cell parameters of the Miura-ori pattern on the qualitative phases of response of the sandwich plate to blast loads as well as on the energy dissipation in the Miura-ori core and facesheets centroidal deflections. It was shown that for a fixed value of side length ( $a$ ) of rhombic unit cells ( $a = b$ ), increasing the dihedral fold angle ( $\theta$ ), which is equivalent to increasing the number of unit cells perpendicular to the corrugation ( $y_m$ ), increases the energy dissipation in the Miura-ori core (Table 3) while not significantly affecting the facesheets centroidal deflections. It should be noted that the thickness of the facets was adjusted to maintain a constant core areal density.

We only consider unit cells with ( $a = b$ ) and set  $H = 5$  mm. For a given number of unit cells  $\{x_m, y_m\}$ , increasing their number along (across) the corrugation,  $x_m$  ( $y_m$ ), reduces the side length  $a$  (the acute angle  $\alpha$ ); see Eqs. (3) and (4). Once  $x_m$  is chosen,  $y_m$  is restricted to be greater than or equal to  $x_m$ . The thickness  $t_s$  of the sheet material is adjusted to maintain the relative core density at  $0.05\rho_m$  (Eq. (5)). For the square honeycomb core, we only consider equal number of webs running in both directions ( $x_m = y_m$ ) and adjust thickness  $t_w$  of the webs to maintain the relative core density at  $0.05\rho_m$ .

In Table 6 we have summarized the 3 unit cell geometries chosen for the two cores, resulting in 12 different two-core sandwich plates whose deformations are analyzed till  $t = 3$  ms for blast loads given by Eq. (1) with  $P_0 = 100$  MPa and 300 MPa.

We have summarized in Tables 7 and 8 the energy dissipated in each core and their sum, the energy dissipated in a core as a fraction of the total energy dissipated in the sandwich structure, and the top and the bottom facesheet centroidal deflections. Based on these results, we make the following observations:

- For each of the four combinations, increasing the number of unit cells  $\{x_m, y_m\}$  increases the total energy dissipated in the cores through plastic deformations (column 5). This change is significantly more in the Miura-ori core sandwich plates than that in the honeycomb core sandwich plates. For example, increasing the number of unit cells from  $\{3, 3\}$  to  $\{7, 7\}$  for  $P_0 = 100$  MPa increases by 135% and 32%, respectively, the energy dissipated by the cores for the Miura-Miura and the honeycomb-honeycomb combinations. Furthermore, the fraction of the total energy dissipated in the structure (column 6), which can be viewed as the efficiency of the cores, significantly increases with an increase in the number of unit cells. Increasing the number of unit cells decreases the side length ( $a$ ) of each fold and increases its stiffness (inversely proportional to  $a^3$ ) and buckling load (inversely proportional to  $a^2$ ). However, to maintain a constant areal density, the thickness of the webs ( $t_w$ ) is decreased which causes a reduction in the area moment of inertia

**Table 6**  
Unit cell geometries of the Miura-ori and honeycomb core models.

Case	$x_m$	$y_m$	Miura-ori				Honeycomb	
			$a$ (mm)	$\alpha$ (degrees)	$\theta$ (degrees)	$t_s$ (mm)	$t_w$ (mm)	
1	3	3	17.401	74.03	17.39	0.239	0.834	
2	5	5	11.180	66.42	29.21	0.218	0.500	
3	7	7	8.719	61.98	40.51	0.190	0.357	

**Table 7**  
Energy dissipated and facesheet centroidal deflections of the two-core sandwich plates for  $P_0 = 100$  MPa.

Case	Combination	PD*	PD	PD	PD	Top facesheet deflection (mm)	Bottom facesheet deflection (mm)
		top (kJ)	bottom (kJ)	cores (kJ)	cores/Total PD		
1	Miura-HC	0.179	0.180	0.360	0.23	14.19	8.94
	HC-Miura	0.195	0.102	0.297	0.24	12.43	8.32
	Miura-Miura	0.190	0.130	0.320	0.19	16.11	8.90
	HC-HC	0.195	0.118	0.313	0.31	9.59	8.93
2	Miura-HC	0.357	0.233	0.590	0.38	13.96	8.36
	HC-Miura	0.230	0.184	0.414	0.35	12.24	7.56
	Miura-Miura	0.349	0.200	0.549	0.33	15.58	8.54
	HC-HC	0.249	0.124	0.373	0.39	9.75	8.45
3	Miura-HC	0.530	0.219	0.749	0.48	13.60	7.71
	HC-Miura	0.242	0.218	0.460	0.40	12.07	7.50
	Miura-Miura	0.513	0.238	0.751	0.45	15.59	6.91
	HC-HC	0.286	0.126	0.412	0.42	9.96	8.31

\*PD = Energy dissipated.

- (proportional to  $t_w^3$ ) and hence, the bending stiffness. Therefore, the aspect ratio of the webs ( $a/t_w$ ) plays an important role in the force required to deform them and on the energy dissipated in the core. The same observations hold for  $P_0 = 300$  MPa, however, the core efficiency is lesser than that for  $P_0 = 100$  MPa and the plastic bending deformations of the facesheets help dissipate a greater fraction of the incident energy.
- The top core that faces the blast load dissipates a greater amount of energy through plastic deformations than the bottom core. For  $P_0 = 100$  MPa, a Miura-ori top core dissipates a greater amount of energy than a honeycomb top core. However, for  $P_0 = 300$  MPa, the honeycomb top core efficiency is greater than that of the Miura-ori core because a larger fraction of the honeycomb webs plastically buckle. In terms of the total energy dissipated in the cores, the Miura-honeycomb and the Miura-Miura combinations perform the best.
  - For  $P_0 = 100$  MPa, the centroidal deflections of the top and the bottom facesheets in each combination decrease with an increase in the number of unit cells. However, the centroidal deflections are not significantly affected for  $P_0 = 300$  MPa. As mentioned in the previous section, the top facesheet bounding a honeycomb core has considerably smaller centroidal deflections than a top facesheet bounding a Miura-ori core. Furthermore, using a Miura-ori core abutting the bottom facesheet helps dissipate a significant fraction of the incident energy and decreases the bottom facesheet centroidal deflections.

These observations indicate the need to establish a compromise between conflicting structural requirements. For designs based on total energy dissipation in the cores, the Miura-honeycomb combination is ideal, particularly for  $P_0 = 100$  MPa. However, from a structural integrity standpoint, the honeycomb-Miura has the least bottom facesheet centroidal deflection and is second only to the honeycomb-honeycomb combination for the top facesheet centroidal deflection.

In order to assess the reliability of the sandwich plates, in Table 9 we have listed the maximum equivalent plastic strain induced in each core for the 12 combinations for  $P_0 = 100$  MPa. We see that the maximum plastic strain in the Miura-ori cores are larger than that in the corresponding honeycomb core combinations. As a result, the Miura-ori-based designs may cause a material point to fail at a lower value of  $P_0$  than the honeycomb-based designs.

Assuming that the deformation process is adiabatic and that the entire energy dissipated through plastic deformations is converted to heat, we have estimated the local temperature rise,  $\Delta T_r$ , in each core

**Table 8**  
Energy dissipated and facesheet centroidal deflections of the two-core sandwich plates for  $P_0 = 300$  MPa.

Case	Combination	PD top (kJ)	PD bottom (kJ)	PD cores	PD cores/ Total PD	Top facesheet deflection (mm)	Bottom facesheet deflection (mm)
1	Miura-HC	0.768	0.848	1.616	0.14	32.26	25.65
	HC-Miura	1.214	0.519	1.733	0.16	30.87	25.25
	Miura-Miura	0.805	0.668	1.473	0.13	33.68	25.68
	HC-HC	1.208	0.797	2.005	0.19	29.48	25.33
2	Miura-HC	1.376	1.262	2.638	0.24	32.73	25.50
	HC-Miura	1.719	0.849	2.568	0.23	31.55	24.96
	Miura-Miura	1.362	1.077	2.438	0.21	34.09	26.26
	HC-HC	1.741	0.924	2.665	0.25	30.37	25.43
3	Miura-HC	1.850	1.424	3.274	0.29	32.93	25.26
	HC-Miura	2.014	1.193	3.207	0.28	32.07	24.58
	Miura-Miura	1.943	1.259	3.202	0.28	34.07	25.12
	HC-HC	2.118	1.033	3.151	0.29	31.20	25.36

**Table 9**  
Maximum plastic strain, local temperature rise and magnitude of the peak overall reaction forces in the two-core sandwich plates for  $P_0 = 100$  MPa.

Case	Combination	$\epsilon_p$ cores		$\Delta T_r$ (K) cores		RF* (kN)
		Top	Bottom	Top	Bottom	
1	Miura-HC	0.724	0.277	180.2	33.7	193.7
	HC-Miura	0.382	0.434	57.9	72.2	118.9
	Miura-Miura	0.792	0.654	212.3	149.8	230.4
	HC-HC	0.489	0.258	89.0	30.0	92.8
2	Miura-HC	1.023	0.530	341.9	102.7	183.9
	HC-Miura	0.509	0.743	95.5	189.0	119.7
	Miura-Miura	0.917	0.804	278.8	218.5	211.6
	HC-HC	0.562	0.299	113.8	38.1	98.2
3	Miura-HC	1.361	0.581	585.9	120.9	170.8
	HC-Miura	0.600	1.157	128.4	430.8	119.6
	Miura-Miura	1.235	0.989	487.3	321.1	198.2
	HC-HC	0.688	0.336	164.0	46.5	103.9

\*RF = Peak overall reaction force along an edge.

(columns 5 and 6 of Table 9) as  $\Delta T_r = ((\sigma_y + E_r \cdot \epsilon_p) \cdot \epsilon_p) / (2 \cdot \rho_m \cdot c)$ , where  $c = 450$  J/kg K is the specific heat of the steel. At the end of the deformation process, the rise in the maximum local temperature is larger in the Miura-ori cores than that in the honeycomb cores indicating that effects of thermal softening and thermal stresses may play important roles in these core geometries. The consideration of thermal softening can induce localization of deformations into narrow regions of intense plastic deformations, usually called adiabatic shear bands, that are precursors to cracking; e.g., see [54].

The magnitudes of the peak overall reaction forces along edges of the top facesheets are listed in the last column of Table 9, for  $P_0 = 100$  MPa. The asymmetry of the Miura-ori core causes unequal reaction forces at the longitudinal edges,  $x = 0$  and  $x = 100$  mm, and only the maximum total reaction force on an edge is provided. For the honeycomb core, the total reaction force on each edge was the same. Using a Miura-ori core at the top leads to higher reaction forces at the longitudinal edges of the top facesheet than that when using a honeycomb core. The maximum equivalent plastic strain in the facesheets were observed at the center of the longitudinal edges, i.e., at (0, 50) and (100, 50) mm indicating that failure would initiate at these locations, with the top facesheet failing first.

**5. Influence of a blast shield on deformations of the honeycomb-Miura sandwich plate**

We now study effects of a rigidly clamped blast shield, constructed as a  $100 \times 100 \times 1.5$  mm 4340 steel plate, on the blast performance of a

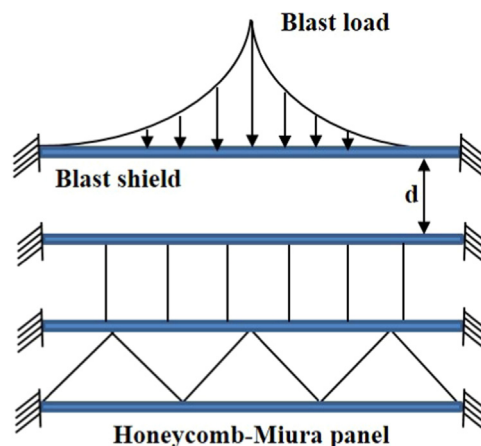


Fig. 16. Design of a blast shield.

sandwich structure (see Fig. 16). The high-intensity dynamic loads specified by Eq. (1) were applied on its top surface. The shield was discretized with  $60 \times 60 \times 3$  uniform C3D8R elements. We consider the honeycomb-Miura combination with {7, 7} unit cells (case 3 in Table 6), facesheet thickness  $h_f = 1.5$  mm, core thickness  $H = 5$  mm and a standoff distance  $d$  from the shield. The general contact algorithm in ABAQUS was employed to define frictionless contact between all surfaces. The blast overpressure  $P_0$  is varied from 50 MPa to 400 MPa and  $d$  from 1 mm to 5 mm. Comparisons are carried out with equal-weight sandwich panels without a shield wherein the thickness of the facesheets  $h_f = 2$  mm with other geometric parameters the same as in the structure with the blast shield. The shield deflects and its points touch the top facesheet thereby transferring the load. Because of the asymmetry of the honeycomb-Miura webs, the reactions between the blast shield and the top facesheet are not uniformly distributed around the shield centroid. Large equal and opposite values of  $\sigma_{zz}$  at adjoining points of the facesheet suggest large local bending with curvature changes in those regions.

Based on the results computed till  $t = 3$  ms, Fig. 17 depicts the energy dissipation in the cores as a fraction of the total energy dissipated in the sandwich structure (PD) and the bottom facesheet centroidal displacements ( $w_b$ ) of the honeycomb-Miura sandwich plate. At a particular loading intensity, increasing  $d$  reduces the energy dissipated by the cores indicating an increase in the load-carrying capacity of the sandwich panel with a shield. Under the assumption that the stresses are proportional to  $P_0$ , the plastic energy dissipated in the structure will be proportional to  $P_0^2$  and the increase in the load-carrying capacity may be estimated as  $(\sqrt{\frac{PD_{withoutshield}}{PD_{withshield}}} - 1)$ , which for  $P_0 = 100$  MPa and  $d = 5$  mm is 19.5%. Alternatively, the weight savings for a specified

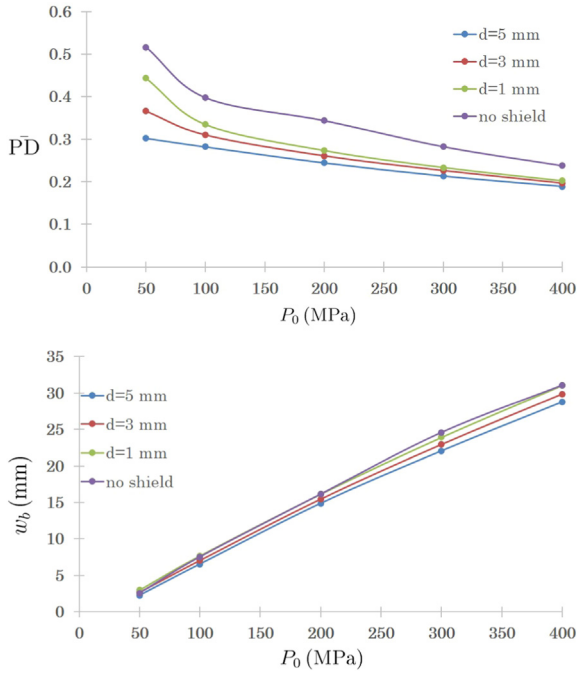


Fig. 17. Energy dissipation in the cores as a fraction of the total energy dissipated in the sandwich structure (PD) and the bottom facesheet centroidal displacement ( $w_b$ ) of the honeycomb-Miura sandwich plate.

loading intensity can be estimated as  $\left(1 - \frac{PD_{withshield}}{PD_{withoutshield}}\right)$ , which for the  $d = 5$  mm case and  $P_0 = 50$  MPa and  $P_0 = 400$  MPa is 42% and 21%, respectively. Using a blast shield reduces the bottom facesheet centroidal deflections (see Fig. 17), particularly at higher loading intensities. For example, for  $P_0 = 300$  MPa and  $d = 5$  mm, the bottom facesheet centroidal deflections are reduced by 10% when compared to the panel without the shield. Increasing the standoff distance of the

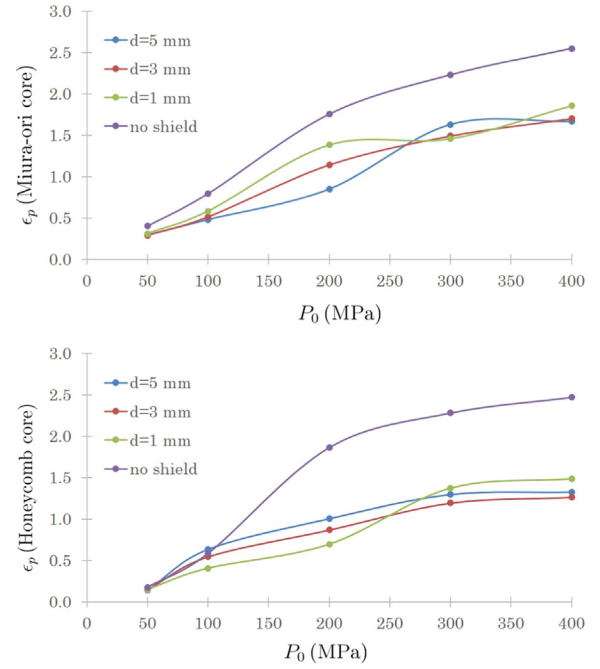


Fig. 19. Equivalent plastic strain at critical locations in the Miura-ori and honeycomb cores.

shield increases the load carrying capacity while reducing the bottom facesheet centroidal deflections.

In Fig. 18, for  $P_0 = 100$  MPa, we have shown contour plots of the  $\sigma_{zz}$  stress on the outer surface of the top facesheet at four times for  $d = 1$  mm and  $d = 5$  mm to demonstrate the qualitative difference in the load transfer between the shield and the top facesheet for the two cases. Increasing  $d$  delays the transfer of the blast load to the top facesheet (from  $t = 0.03$  ms for  $d = 1$  mm to  $t = 0.06$  ms for  $d = 5$  mm),

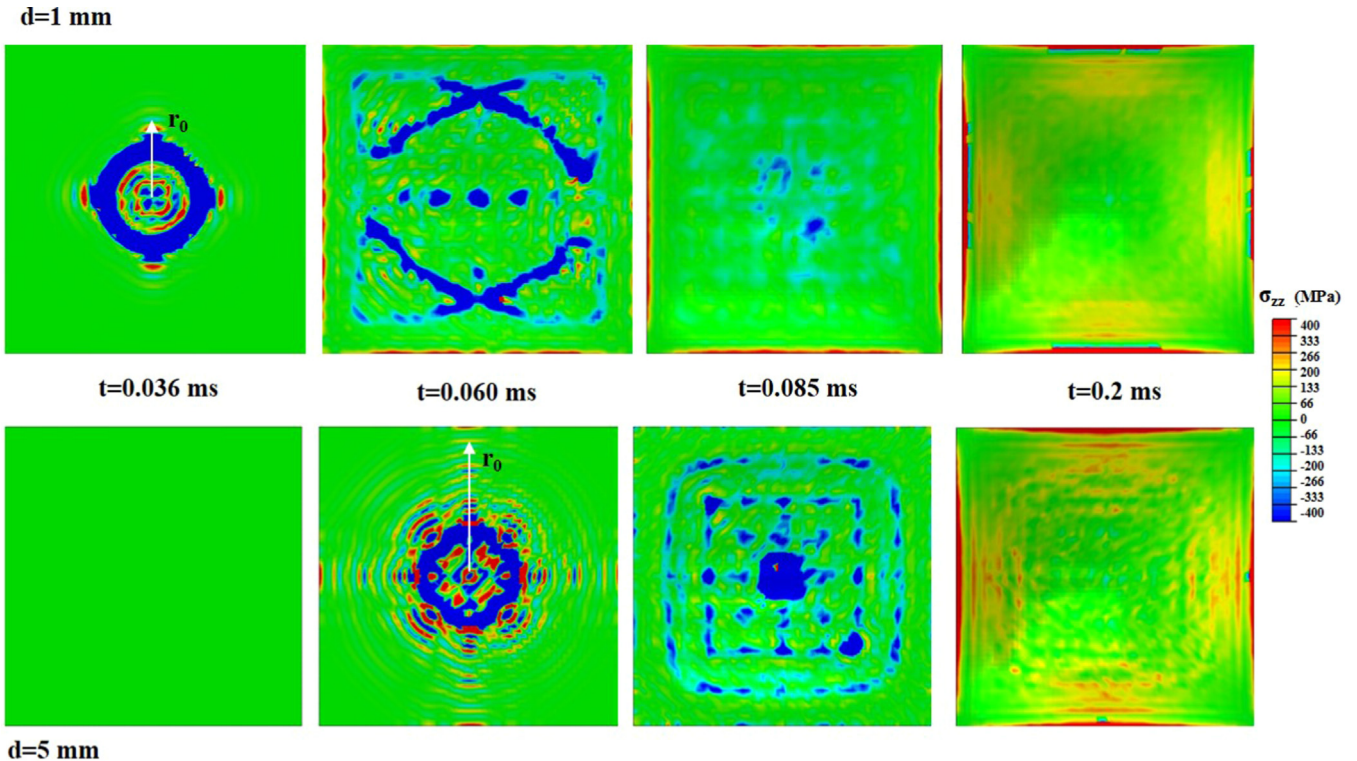


Fig. 18.  $\sigma_{zz}$  contour plots on the outer surface of the top facesheet (100\*100 mm) of the honeycomb-Miura sandwich plate at four times for  $d = 1$  mm and  $d = 5$  mm.

and alters the area where the maximum pressure, as indicated by the value of  $\sigma_{zz}$ , acts. As determined by the radius of the outermost contour,  $r_0$ , in the figure, the initial load transferred (at  $t = 0.03$  ms for  $d = 1$  mm and at  $t = 0.06$  ms for  $d = 5$  mm) is distributed over a larger surface area of the top facesheet for the  $d = 5$  mm case.

For the case without the shield, locations of the maximum equivalent plastic strain in the Miura-ori and the honeycomb cores were determined for different load intensities. Fig. 19 depicts the equivalent plastic strain,  $\epsilon_p$ , at these locations for various standoff distances. Consistent with our previous observation of a reduction in the energy dissipated in the cores by using a blast shield, the maximum equivalent plastic strain in the cores is significantly reduced thereby improving the integrity of the structure. For example, for  $P_0 = 200$  MPa, the plastic strain at the critical locations in the Miura-ori and the honeycomb cores (determined from the panel without the shield) were reduced by 52% and 46%, respectively, when a blast shield was used at  $d = 5$  mm. As the standoff distance is reduced, the maximum equivalent plastic strain in the Miura-ori core increases since the load transferred to the sandwich panel from the shield becomes localized. At higher loading intensities ( $P_0 > 200$  MPa), a larger fraction of the honeycomb webs buckle plastically which increases the energy dissipated by plastic deformations in the honeycomb core, particularly for  $d = 1$  mm. The optimum value of  $d$  that minimizes the maximum value of  $\epsilon_p$  depends upon the core combination and  $P_0$ .

## 6. Remarks

The numerical tests conducted in this paper serve as a useful guideline for researchers to design prototypes of a particular hybrid core design based on application requirements. Nevertheless, it is important to validate these numerical findings with experimental results. This would help to delineate effects of imperfections introduced during the manufacturing process as well as of the crease-weakening during the folding of the core, on the performance of Miura-ori/honeycomb core hybrid sandwich plates. A number of experimental studies have been conducted on the quasi-static response [29,18,24,23] and low-velocity impact behavior [20,21] of origami core sandwich plates.

By using a synchronous folding method developed by Schenk et al. [52], Miura-ori prototypes can be quickly produced with minimal tooling and blast experiments, similar to those on honeycomb core sandwich plates [17,9], can be conducted to validate the numerical results. Batra's research laboratory does not have experimental facilities and Virginia Tech does not have a range to test structures under blast loads.

We [26] verified the capability of the software ABAQUS/ Explicit to accurately predict high-intensity dynamic deformations of sandwich plates by simulating the test configurations of Dharmasena et al. [9]. The simulations well captured the large structural deformations including the buckling of the webs. New paragraph One can alternatively use a cellular design detailed in [55] for designing lightweight impact resistant structures. Li et al. [56] have recently studied the crushing behavior of folded kirigami structure with square dome shape.

## 7. Conclusions

We have numerically analyzed, with and without a bumper shield, the transient response of two-core sandwich plates constructed using combinations of equal areal density Miura-ori and honeycomb cores. The cores are not replaced by equivalent monolithic structures of homogeneous materials.

For one configuration, the total energy dissipated and the facesheet maximum deflections with and without using a material damage and failure model are found to be essentially the same. Thus, all other simulations have been conducted without considering the material failure.

Design studies on two-core plates without a shield have been

conducted to delineate the influence of the unit cell parameters of the Miura-ori and the honeycomb core on the energy dissipated by the cores and the facesheet deflections. Increasing the number of unit cells from {3, 3} to {7, 7} for moderate loads increases the energy dissipated in the Miura-Miura and the honeycomb-honeycomb cores by 135% and 32%, respectively.

For hybrid core sandwich plates, it is found that using a Miura-ori core at the top helps dissipate considerably more energy through plastic deformations than using a honeycomb core, particularly for moderate blast intensities. For designs based on minimizing facesheet deflections and the total reaction forces at the supports, the honeycomb-Miura combination is effective.

Comparisons carried out for equal areal density structures with and without a blast shield indicate that using a bumper significantly increases the load-carrying capacity of the structure. Alternatively, significant weight-savings can be achieved along with a reduction in the bottom facesheet centroidal deflections and the maximum equivalent plastic strain induced in the cores.

## Acknowledgments

RCB's work was partially supported by the US Office of Naval Research grant N00014-16-1-2309 to Virginia Polytechnic Institute and State University with Dr. Y.D.S. Rajapakse as the program manager. Views expressed in the paper are those of the authors and neither of ONR nor of Virginia Tech. We are indebted to the anonymous reviewers and the editor-in-chief for their suggestions that have improved upon the quality and presentation of the work.

## References

- [1] L.J. Gibson, M.F. Ashby, Cellular Solids: Structure and Properties, Cambridge university press, 1999.
- [2] Z. Xue, J.W. Hutchinson, Preliminary assessment of sandwich plates subject to blast loads, *Int. J. Mech. Sci.* 45 (4) (2003) 687–705.
- [3] J.W. Hutchinson, Z. Xue, Metal sandwich plates optimized for pressure impulses, *Int. J. Mech. Sci.* 47 (4) (2005) 545–569.
- [4] Z. Xue, J.W. Hutchinson, Crush dynamics of square honeycomb sandwich cores, *Int. J. Numer. Methods Eng.* 65 (13) (2006) 2221–2245.
- [5] F. Zhu, Z. Wang, G. Lu, G. Nurick, Some theoretical considerations on the dynamic response of sandwich structures under impulsive loading, *Int. J. Impact Eng.* 37 (6) (2010) 625–637.
- [6] Z. Xue, J.W. Hutchinson, A comparative study of impulse-resistant metal sandwich plates, *Int. J. Impact Eng.* 30 (10) (2004) 1283–1305.
- [7] G. McShane, D. Radford, V. Deshpande, N. Fleck, The response of clamped sandwich plates with lattice cores subjected to shock loading, *Eur. J. Mech.-A/Solids* 25 (2) (2006) 215–229.
- [8] G. McShane, V. Deshpande, N. Fleck, The underwater blast resistance of metallic sandwich beams with prismatic lattice cores, *J. Appl. Mech.* 74 (2) (2007) 352–364.
- [9] K.P. Dharmasena, H.N. Wadley, Z. Xue, J.W. Hutchinson, Mechanical response of metallic honeycomb sandwich panel structures to high-intensity dynamic loading, *Int. J. Impact Eng.* 35 (9) (2008) 1063–1074.
- [10] F. Zhu, L. Zhao, G. Lu, Z. Wang, Deformation and failure of blast-loaded metallic sandwich panels- experimental investigations, *Int. J. Impact Eng.* 35 (8) (2008) 937–951.
- [11] F. Zhu, L. Zhao, G. Lu, E. Gad, A numerical simulation of the blast impact of square metallic sandwich panels, *Int. J. Impact Eng.* 36 (5) (2009) 687–699.
- [12] D. Karagiozova, G. Nurick, G. Langdon, S.C.K. Yuen, Y. Chi, S. Bartle, Response of flexible sandwich-type panels to blast loading, *Compos. Sci. Technol.* 69 (6) (2009) 754–763.
- [13] D. Karagiozova, G. Nurick, G. Langdon, Behaviour of sandwich panels subject to intense air blasts-Part 2: numerical simulation, *Compos. Struct.* 91 (4) (2009) 442–450.
- [14] G. Nurick, G. Langdon, Y. Chi, N. Jacob, Behaviour of sandwich panels subjected to intense air blast-Part 1: experiments, *Compos. Struct.* 91 (4) (2009) 433–441.
- [15] K.P. Dharmasena, H.N. Wadley, K. Williams, Z. Xue, J.W. Hutchinson, Response of metallic pyramidal lattice core sandwich panels to high intensity impulsive loading in air, *Int. J. Impact Eng.* 38 (5) (2011) 275–289.
- [16] G. Imbalzano, P. Tran, T.D. Ngo, P.V. Lee, A numerical study of auxetic composite panels under blast loadings, *Compos. Struct.* 135 (2016) 339–352.
- [17] H. Rathbun, D. Radford, Z. Xue, M. He, J. Yang, V. Deshpande, N. Fleck, J. Hutchinson, F. Zok, A. Evans, Performance of metallic honeycomb-core sandwich beams under shock loading, *Int. J. Solids Struct.* 43 (6) (2006) 1746–1763.
- [18] S. Heims, J. Cichosz, M. Klaus, S. Kilchert, A. Johnson, Sandwich structures with textile-reinforced composite foldcores under impact loads, *Compos. Struct.* 92 (6) (2010) 1485–1497.

- [19] A. Lebé, K. Sab, Transverse shear stiffness of a chevron folded core used in sandwich construction, *Int. J. Solids Struct.* 47 (18) (2010) 2620–2629.
- [20] J. Gattas, Z. You, Quasi-static impact of indented foldcores, *Int. J. Impact Eng.* 73 (2014) 15–29.
- [21] J. Gattas, Z. You, The behaviour of curved-crease foldcores under low-velocity impact loads, *Int. J. Solids Struct.* 53 (2015) 80–91.
- [22] R. Fatters, J. Gattas, Z. You, Quasi-static crushing of eggbox, cube, and modified cube foldcore sandwich structures, *Int. J. Mech. Sci.* 101 (2015) 421–428.
- [23] X. Zhou, H. Wang, Z. You, Mechanical properties of Miura-based folded cores under quasi-static loads, *Thin-Walled Struct.* 82 (2014) 296–310.
- [24] S. Liu, G. Lu, Y. Chen, Y.W. Leong, Deformation of the Miura-ori patterned sheet, *Int. J. Mech. Sci.* 99 (2015) 130–142.
- [25] M. Schenk, S. Guest, G. McShane, Novel stacked folded cores for blast-resistant sandwich beams, *Int. J. Solids Struct.* 51 (25) (2014) 4196–4214.
- [26] A. Pydah, R. Batra, Crush dynamics and transient deformations of elastic-plastic Miura-ori core sandwich plates, *Thin-Walled Struct.* 115 (2017) 311–322.
- [27] C. Weeks, C. Sun, Multi-core composite laminates, *J. Adv. Mater.* 25 (3) (1994) 28–37.
- [28] B. Cao, B. Hou, Y. Li, H. Zhao, An experimental study on the impact behavior of multilayer sandwich with corrugated cores, *Int. J. Solids Struct.* 109 (2017) 33–45.
- [29] S. Heimbs, P. Middendorf, S. Kilchert, A.F. Johnson, M. Maier, Experimental and numerical analysis of composite folded sandwich core structures under compression, *Appl. Compos. Mater.* 14 (5–6) (2007) 363–377.
- [30] Z. Wang, Q. Xu, Experimental research on soundproof characteristics for the sandwich plates with folded core, *J. Vib. Eng.* 19 (1) (2006) 65–69.
- [31] A. Pydah, R. Batra, Analytical solution for cylindrical bending of two-layered corrugated and webcore sandwich panels, *Thin-Walled Struct.* 123 (2018) 509–519.
- [32] F. Whipple, Possible Hazards to a Satellite Vehicle, Project RAND, Douglas Aircraft Corporation, Santa Monica, California.
- [33] A.E. Olshaker, Experimental Investigation in Lead of the Whipple “Meteor Bumper”, *J. Appl. Phys.* 31 (12) (1960) 2118–2120.
- [34] R. Wallace, Effects of hypervelocity particles on shielded structures, *ARS J.* 32 (8) (1962) 1231–1237.
- [35] L. Chhabildas, E. Hertel, S. Hill, Hypervelocity impact tests and simulations of single Whipple bumper shield concepts at 10 km/s, *Int. J. Impact Eng.* 14 (1–4) (1993) 133–144.
- [36] E.L. Christiansen, Design and performance equations for advanced meteoroid and debris shields, *Int. J. Impact Eng.* 14 (1) (1993) 145–156.
- [37] M. Katayama, S. Kibe, S. Toda, A numerical simulation method and its validation for debris impact against the whipple bumper shield, *Int. J. Impact Eng.* 17 (4) (1995) 465–476.
- [38] E.A. Taylor, M. Herbert, B. Vaughan, J. McDonnell, Hypervelocity impact on carbon fibre reinforced plastic/aluminium honeycomb: comparison with Whipple bumper shields, *Int. J. Impact Eng.* 23 (1) (1999) 883–893.
- [39] D.C. Hofmann, L. Hamill, E. Christiansen, S. Nutt, Hypervelocity impact testing of a metallic glass-stuffed Whipple shield, *Adv. Eng. Mater.* 17 (9) (2015) 1313–1322.
- [40] S. Ashley, Safety in the sky: designing bomb-resistant baggage contain, *Mech. Eng.* 114 (6) (1992) 81.
- [41] X. Dang, P.C. Chan, Design and test of a blast shield for boeing 737 overhead compartment, *Shock Vib.* 13 (6) (2006) 629–650.
- [42] V. ABAQUS, 6.14 Documentation, Dassault Systemes Simulia Corporation.
- [43] R. Batra, N. Hassan, Response of fiber reinforced composites to underwater explosive loads, *Compos. Part B: Eng.* 38 (4) (2007) 448–468.
- [44] R.H. Cole, Underwater Explosions, Dover Publications, 1965.
- [45] M. Schenk, S.D. Guest, Geometry of Miura-folded metamaterials, *Proc. Natl. Acad. Sci. USA* 110 (9) (2013) 3276–3281.
- [46] G.R. Johnson, W.H. Cook, Fracture characteristics of three metals subjected to various strains, strain rates, temperatures and pressures, *Eng. Fract. Mech.* 21 (1) (1985) 31–48.
- [47] Y. Wen, C. Xu, Y. Jin, R. Batra, Rifle bullet penetration into ballistic gelatin, *J. Mech. Behav. Biomed. Mater.* 67 (2017) 40–50.
- [48] A. Chadevani, K.A. Iyer, D.S. Mehoke, R.C. Batra, Hypervelocity impact of a steel microsphere on fused silica sheets, *Int. J. Impact Eng.* 80 (2015) 116–132.
- [49] C.E. Anderson, T.J. Holmquist, Application of a computational glass model to compute propagation of failure from ballistic impact of borosilicate glass targets, *Int. J. Impact Eng.* 56 (2013) 2–11.
- [50] C.E. Anderson, T.J. Holmquist, Computational modeling of failure for hypervelocity impacts into glass targets, *Procedia Eng.* 58 (2013) 194–203.
- [51] R. Batra, Z. Wei, Dynamic buckling of a thin thermoviscoplastic rectangular plate, *Thin-walled Struct.* 43 (2) (2005) 273–290.
- [52] M. Schenk, J. Allwood, S. Guest, Cold gas-pressure folding of Miura-ori sheets, in: *Proceedings of International Conference on Technology of Plasticity (ICTP 2011)*, Sept, 25–30, 2011.
- [53] Z. Wei, J.L. Yu, R.C. Batra, Dynamic buckling of thin cylindrical shells under axial impact, *Int. J. Impact Eng.* 32 (2006) 947–967.
- [54] R.C. Batra, L. Chen, Effect of viscoplastic relations on the instability strain, shear band initiation strain, the strain corresponding to the minimum shear band spacing, and the band width in thermoviscoplastic materials, *Int. J. Plasticity* 17 (2001) 1465–1489.
- [55] D. Snelling, Q. Li, N. Meisel, C.B. Williams, R.C. Batra, A.P. Druschitz, Lightweight metal cellular structures fabricated via 3D printing and sand case molds, *Adv. Eng. Mater.* 17 (2015) 923–932.
- [56] Z. Li, W. Chen, H. Hao, Crushing behaviours of folded kirigami structure with square dome shape, *Int. J. Impact Eng.* 115 (2018) 94–105.